Published in final edited form as:
Brain Res. 2008 October 31; 1238: 163–171. doi:10.1016/j.brainres.2008.08.031.

Neuronal and Astrocytic Apoptosis after Subarachnoid Hemorrhage:

A Possible Cause for Poor Prognosis

Mohammed Sabri, **Ayako Kawashima, M.D.**, **Jinglu Ai, Ph.D.**, and **R. Loch Macdonald, M.D., Ph.D.**
Division of Neurosurgery, St. Michael's Hospital, Keenan Research Centre in the Li Ka Shing Knowledge Institute of St. Michael's Hospital and Department of Surgery, University of Toronto, Toronto, Ontario, Canada

Abstract

Clinical evidence suggests that factors other than cerebral vasospasm, such as delayed neuronal and astrocytic cell death, may play a role in the poor prognosis of patients with subarachnoid hemorrhage (SAH). Here we examined this using immunohistochemistry and confocal microscopy in 3 different brain areas in a dog model of SAH. Using antibodies against neuronal marker neuronal nuclear protein (NeuN) and astrocyte marker glial fibrillary acidic protein (GFAP) in conjunction with apoptosis marker (cleaved caspase-3), we quantified neurons and astrocytes to monitor the degree of apoptosis in both groups. Experimental SAH group showed 44 ± 1% caspase-3 positive neurons in comparison to the 2.0 ± 0.1% in the control group ($P < 0.001$, 6 animals each group). For astrocytes, a total 25 ± 1% were caspase-3 positive in day 7 SAH group, as compared to 0.40 ± 0.01% for controls ($P < 0.001$). Regional analysis revealed that neuronal caspase-3 immunoreactivity in all 3 regions were significantly higher ($P < 0.001$) in SAH animals than that in the control animals. However, the analysis of total area, size and signal co-localization of GFAP with caspase-3 indicated that astrocytic reactivity and proliferation are seen primarily in the hippocampal area, with the least changes detectable in the brainstem. We conclude that in the dog model, there was a significant increase of neuronal and astrocytic cleaved caspase-3, possibly reflecting apoptosis, following SAH induction. These changes coupled with neurological deterioration seen in patients may present a possible reason for the poor outcome in SAH patients.

Keywords

Apoptosis; astrocyte; cerebral vasospasm; neuron; subarachnoid hemorrhage

1. INTRODUCTION

Subarachnoid hemorrhage (SAH) is a type of stroke characterized by bleeding into the subarachnoid space spontaneously or due to trauma. Spontaneous cases are most commonly due to rupture of an intracranial aneurysm. Although only 7% of strokes are due to SAH, death

Correspondence and Reprint Requests: R. Loch Macdonald, M.D., Ph.D., Division of Neurosurgery, St. Michael's Hospital, 30 Bond Street, Toronto, Ontario, Canada M5B 1W8, Phone: (416) 864 5452, Fax: (416) 864 5634, Email: Macdonaldlo@smh.toronto.on.ca.

is more common after SAH than after other types of stroke, the average age is younger, and outcome among survivors is particularly dismal (Ingall and Whisnant, 1998; Taylor et al., 1996). A major cause of death and disability among patients with aneurysmal SAH is cerebral vasospasm (Dorsch and King, 1994; Kassell et al., 1990). Cerebral vasospasm is transient, delayed constriction of cerebral arteries that occurs in 70% of SAH patients 3 to 12 days after SAH and lasts about 2 weeks (Weir, 1995). If vasospasm is severe enough, it can cause cerebral infarction in the territory of the spastic artery, which can cause neurological deterioration and poor outcome (Nolan and Macdonald, 2006). Some patients, however, deteriorate neurologically after SAH and do not have vasospasm. Furthermore, preventing or reversing vasospasm does not always improve outcome (Macdonald et al., 2006).

Other processes such as microcirculatory changes, thromboembolism, delayed neuronal and astrocytic apoptosis and cortical spreading depression have been considered as possible causes of delayed brain injury after SAH (Hansen-Schwartz et al., 2007; Macdonald et al., 2007). Few experimental data exist to document whether or not these processes occur after SAH. The goal of this study was to assess neuronal and astrocyte injury after SAH in a dog model. While detecting neuronal injury after SAH would be accepted as important, the rationale for studying astrocytes may be less evident but there is emerging evidence that astrocyte damage contributes to neuronal death (Haydon and Carmignoto, 2006; Ouyang et al., 2007).

2. RESULTS

2.1 Angiographic Vasospasm

There was a 56 ± 11% reduction in basilar artery diameter 7 days after SAH ($p = 0.0043$). Control animals had a 6 ± 4% decrease in basilar artery diameter 7 days after physiologic saline injection ($p = 0.66$). There were no significant changes in body weight, blood pressure, heart rate, body temperature, arterial oxygen and carbon dioxide content between control and SAH animals at baseline or within groups between days 0 and 7 (data not shown).

2.2 Quantitation of Neuronal Changes

Possible neuronal apoptosis was detected by double-immunofluorescent staining of neurons with antibodies to NeuN and active, cleaved caspase-3 and by terminal deoxynucleotidyl transferase-mediated deoxyuridine triphosphate nick-end labeling (TUNEL). There was no anti-caspase 3 immunoreactivity in NeuN stained neurons from control dogs (Figs. 1A to 1C). In contrast, a significant number of cells showed co-localization of NeuN and anti-caspase-3 in sections from dogs with SAH (Figs. 1D to 1F). Decreased NeuN fluorescence was noted in sections from dogs with SAH (Fig. 1D) compared to the intensity of fluorescence in the control sections, suggesting decreased NeuN expression in neurons after SAH. In addition, the NeuN staining pattern differed in that in control animals there tended to be a smoothly stained cellular surface (Figs. 1A and 1C). In sections from animals with SAH, there was evidence of neuronal shrinkage and apoptotic debris was seen (Figs. 1D and 1F). Cleaved caspase-3 immmunoreactivity was observed in the CA1 region of the hippocampus, as well as adjacent areas, and was qualitatively less in the dentate gyrus. In the cortex, immunoreactivity was seen relatively equally in all layers. There was no TUNEL staining in control dog hippocampus or cortex but after SAH, TUNEL-positive nuclei were seen in both areas and as with cleaved caspase-3, was more frequent in the hippocampus than the dentate gyrus (Fig. 2). Some cells in the hippocampus CA1 region that were positive appeared to be neurons based on morphology (Fig. 2F). TUNEL staining was more prominent in layers 2 to 4 of the cortex and more cells were TUNEL-positive than were positive for cleaved caspase-3.

We quantified 2075 NeuN-positive cells, which will be referred to as neurons, from 3 brain areas (hippocampus, cortex and brainstem) from 7 control and 7 SAH animals. In general, there

were an equal number of total neurons observed in each group (920 for controls and 1155 for SAH, $p = 0.00025$, Fig. 3A). The mean total number of neurons in each of the 3 brain regions per dog also was similar between the 2 groups (193 ± 16 for controls and 152 ± 18 for SAH, $p = 0.00058$, Fig 3A). However, the SAH group had significantly more caspase-3 positive neurons. Total caspase-3 positive neurons from all 3 regions per dog was 84 ± 5 in the SAH group and 3.5 ± 2.4 in controls ($p = 0.000088$, Fig. 3A). This translated into a significantly higher percentage of caspase-3 positive neurons in the SAH group (44 ± 1% of 1155 neurons) compared to the control group (2.0 ± 0.1% of 920 neurons, $p = 0.000065$, Student's t-test, Fig. 3B).

Regional analysis of co-localization of NeuN and caspase-3 staining revealed that the number of labeled neurons was significantly higher in animals with SAH than in the control animals in all 3 regions examined (Fig. 3B, $p = 0.00071$). Also, a significantly higher proportion of neurons were labeled in the hippocampus (48 ± 5%) and cortex (51 ± 3%) of the dogs with SAH than in the brainstem (18 ± 1%, Fig. 3B, $p = 0.000011$, ANOVA). There was no significant difference in the total number of neurons detected and counted between control and SAH animals in each of the 3 brain regions (data not shown).

2.3 Quantitation of Astrocyte Changes

Possible astrocyte apoptosis was assessed using double immunofluorescent staining for glial fibrillary acidic protein (GFAP) and activated caspase-3. In the hippocampus, there was only scant GFAP immunoreactivity in sections from the control animals (Fig. 4A). There was no caspase-3 immunoreactivity and thus no co-localization of it with GFAP in the control animals (Figs. 4B and 4C). In contrast, there was strong GFAP staining (Fig. 4D) and some caspase-3 immunoreactivity (Fig. 4E) in the cortex from animals with SAH (Fig. 4E). Double labeling showed colocalization of caspase-3 with GFAP staining, suggesting apoptotic astrocytes (Fig. 4F). There was a similar pattern of GFAP and anti-caspase-3 positive staining in cortex (Fig. 4G-4L) and brain stem for the two experimental groups.

We quantified the total area of GFAP signal and its co-localization with caspase-3 positive immunoreactivity in hippocampus, cortex and brain stem (Fig. 5). There was a significant increase in total GFAP positive area (257 ± 63 for SAH animals versus 144 ± 33 for controls, Fig. 5A, $p = 0.039$) as well as GFAP/caspase-3 co-localization in the SAH group as compared to controls (84 ± 22 for SAH versus 0.7 ± 0.2 for control, $p = 0.000073$). Regional analysis showed a similar increase in GFAP staining in the hippocampus (89 ± 45 for SAH versus 41 ± 24 for control, $p = 0.046$) and cortex (147 ± 19 for SAH versus 84 ± 45 for control) in the SAH group (Fig. 5B). On the other hand, there was no significant increase of GFAP stained area in the brain stem in the SAH group compared to control (21 ± 14 for SAH compared to 20 ± 10 for control, $p = 0.17$). This suggests there was more reactive astrocytosis and thus greater astrocyte stress in the hippocampus and cortex than in the brain stem after SAH.

Double staining for GFAP and caspase-3 demonstrated a significant increase in brainstem, cortex and hippocampus sections in SAH animals compared to controls (Fig. 5C, $p = 0.00088$). There also were significant differences among each of these regions within the SAH animals (Fig. 5C, $p = 0.018$, ANOVA). The highest percentage of GFAP/caspase-3 colocalization was in the hippocampus (20 ± 6%) followed by cortex (9 ± 3%) and then brainstem (3 ± 1%).

3. DISCUSSION

Aneurysmal SAH causes at least 3 pathophysiologically-important processes: transient global ischemia due to increased intracranial pressure, acute hypertension and deposition of subarachnoid blood clot. Transient ischemia probably only develops in the subgroup of patients that loose consciousness when the aneurysm ruptures (Hop et al., 1999). Acute intracranial and

systemic hypertension contribute to blood brain barrier disruption and cerebral edema (Peterson and Cardoso, 1983; Sasaki et al., 1985). These interact with the subarachnoid clot to produce cerebral vasospasm and possibly various secondary processes (Cahill et al., 2006; Macdonald et al., 2007).

To be important, however, these processes must contribute to brain dysfunction. This could be by causing confluent brain infarction, selective neuronal death by one of the many mechanisms of cell death or dysfunction without cell death (Corbett and Nurse, 1998). Traditionally, large artery vasospasm has been considered a primary factor causing infarction and poor outcome, yet recent studies suggest alleviating vasospasm may not translate into improved outcome (Macdonald et al., 2007). One possible reason is that other processes injure neurons after SAH.

The dog model used here produced severe vasospasm with an average 56% reduction in basilar artery diameter 7 days after SAH. On the other hand, no cerebral infarctions were detected histologically. This is not surprising given the extensive collateral circulation present in dog brain. Prior studies did not demonstrate reduced cerebral blood flow after SAH in dogs (Diringer et al., 1991; Stoodley et al., 2000). In another experiment using the same dog SAH model, we found 15% reduction in MCA diameter 7 days after SAH (Yarnitsky et al., 2005). Therefore, vasospasm is unlikely to be the cause of pathologic changes described here.

In spite of a lack of infarction, extensive neuronal and astrocyte caspase-3 immunoreactivity, a possible marker of apoptosis, was detected. Every animal examined had labeled cells, unlike more limited changes found in rodent models (Prunell et al., 2005). Light microscopic examination of the hippocampus and dentate gyrus in patients dying after SAH or global cerebral hypoxia showed apoptosis in the dentate gyrus in both conditions but necrotic cell death in the hippocampus that was more severe after hypoxia than SAH (Nau et al., 2002).

The present data extend prior observations detecting apoptotic neurons acutely after SAH in rat hippocampus and cortex in an endovascular perforation model that causes a combination of increased intracranial pressure and SAH (Endo et al., 2007; Ostrowski et al., 2005; Park et al., 2004; Prunell et al., 2005). First, the present results suggest SAH causes neuronal injury independent of increased intracranial pressure because control animals had saline injections at the same rate as SAH animals. This is consistent with experiments by Matz, et al., who detected deoxyribonucleic acid (DNA) fragmentation and TUNEL-labeled cells in mouse cortex after injection of hemolyzed blood into the subarachnoid space over the cortex (Matz et al., 2000a; Matz et al., 2000b). Injection of hemolyzed blood into the cisterna magna of rabbits, probably without increasing the intracranial pressure, was associated with some neuronal apoptosis but no vasospasm (Wang et al., 2005). In the endovascular perforation model, apoptosis in brain cells of an uncertain type was associated with increased expression of hypoxia-inducible factor-1alpha, VEGF and BNIP3 (Ostrowski et al., 2005). Whether this occurs with SAH independent of increased intracranial pressure is unknown but it is notable that other investigations correlated acute reductions in cerebral blood flow after SAH in rats with the extent of neuronal apoptosis assessed by TUNEL staining (Prunell et al., 2005).

Second, astrocytes were affected by SAH. Prunell, et al., produced SAH with increased intracranial pressure and reduced cerebral blood flow in rats by the endovascular perforation and chiasmatic cistern injection models (Prunell et al., 2005). About 20% of the TUNEL-positive cells were astrocytes and they were predominately located near where the SAH was. There was decreased GFAP reactivity in areas of neuronal TUNEL staining. On the other hand, the present results found increased GFAP immunoreactivity. This was based on coordinated signal-size mediated analysis of GFAP signal because the interconnected appearance of the astrocytic networks made it difficult to count individual cells by manual or imaging methods. A similar method has been used previously to quantify GFAP (bdel-Rahman et al., 2004). In

keeping with results of Prunell, et al., there was increased apoptosis in astrocytes after SAH except that in the dog model, this was predominately in the hippocampus. Whether the increase in GFAP staining was due to reactive hyperplasia or hypertrophy of astrocytes was not determined. The cause of astrocyte caspase-3 immunoreactivity also is unknown, although the same comments above about neuronal death apply.

Among the limitations of this study are that the pathways by which cells were dying were not fully defined. Activated caspase-3 may indicate apoptosis and this was supported by presence of some TUNEL-positive cells, which may be a more specific indicator of apoptosis, since activated caspase-3 may not always indicate a cell is undergoing apoptosis (Carloni et al., 2007). A complete investigation of cell death pathways and why they occur may be warranted as well as studies to determine the functional importance of cell death after SAH. Effects of SAH on other apoptotic pathways were examined in the rat endovascular perforation model (Cahill et al., 2007). The mitochondrial pathway was examined with cytochrome C, the caspase-independent pathway with apoptosis-inducing factor and the caspase-dependent pathway with caspase-3 and caspase-8. Pifithrin alpha treatment decreased mortality, improved behavior, decreased blood-brain barrier breakdown and brain edema. SAH increased phosphorylated p53, cytochrome C, apoptosis-inducing factor and caspase-3 and -8 as detected by Western blotting in multiple brain regions, as well as producing TUNEL staining and neuronal death in cortex and hippocampus. All of these increases were attenuated by pifithrin alpha treatment. The model produces increased intracranial pressure along with SAH so the changes could be due to one or both processes. The longest time examined after SAH was 72 hours and the cell types affected were not described. Also, the drug treatment may have protected against large artery spasm and thereby prevent distal secondary changes.

In summary, these data show in a large animal model that SAH independent of increased intracranial pressure is associated with neuronal and astrocyte cleaved caspase-3 immunoreactivity, suggestive of apoptosis, in hippocampus and cortex. The animals had cerebral vasospasm and in view of prior studies demonstrating no effect of vasospasm on cerebral blood flow in this model, it is suggested that the changes are likely a primary effect of the SAH.

4. EXPERIMENTAL PROCEDURE

4.1 Dog Model of SAH

Our methods for creation of SAH in dogs have been described (Jahromi et al., 2008; Xie et al., 2007). Mongrel dogs of either sex weighing 15-20 kg were randomly divided into a control (n = 7) or an SAH (n = 7) group. Dogs were placed under general anesthesia and underwent baseline cerebral angiography on day 0. Immediately after angiography, dogs were turned prone and the cisterna magna was punctured percutaneously with a spinal needle and 0.3 ml kg^{-1} cerebrospinal fluid was drained after which 0.5 ml kg^{-1} of fresh, autologous, arterial, nonheparinized blood was injected into the cisterna magna at a rate of 5 ml min^{-1}. Cisternal blood injection was repeated on day 2. Control animals underwent injection of 0.9% NaCl instead of blood. Angiography was repeated on day 7 and animals were sacrificed by perfusion with phosphate buffer saline (PBS). Procedures on animals were approved by the Institutional Animal Care Committee.

4.2 Immunofluorescence Microscopy

Brain regions examined were a coronal section through the cerebral hemispheres at the level of the midtemporal lobe containing the hippocampus and cerebral cortex and a cross section of the brainstem through the pons. The first region was cut into right and left hemispheres and then transversely into an inferior half containing the hippocampus and temporal lobe and a

superior half containing the rest of the hemisphere. Regions were fixed in 4% paraformaldehyde and paraffin embedded. Sections 10 μm thick were taken from each of the 6 regions. They were deparaffinized in xylene, hydrated in a decreasing gradient of ethanol and rinsed with PBS and distilled water. Sections were incubated for 20 min in citrate buffer (pH 6.0) which was pre-heated in a water bath to 96°C. They were washed, blocked with PBS containing 10% normal goat serum, 1% bovine serum albumin and 0.1% sodium azide and permeabilized with 0.3% Triton X-100 for 1 hr with gentle rocking.

Primary antibodies for immunofluorescence were goat anti-mouse NeuN (1:400, Invitrogen, Carlsbad, CA), rabbit anti-human active cleaved caspase-3 (1:400, BD Pharmingen, Franklin Lakes, NJ) and mouse anti-human GFAP (1:400, DAKO, Produktionsvej, Denmark). Sections were incubated with primary antibody in PBS with 1% bovine serum albumin for 30-40 min at room temperature followed by washing and application of secondary antibodies. Secondary antibodies were Alexa Fluor 568 goat anti-mouse for NeuN (Invitrogen), Alexa Fluor 488 goat anti-rabbit for caspase-3 (Invitrogen) and goat anti-mouse for GFAP.

We performed double labeling for NeuN/caspase 3 to detect neuronal apoptosis, and GFAP/caspase-3 to detect astrocyte apoptosis. 4′,6-diamidino-2-phenylindole (DAPI) was used to counterstain nuclei as previously described (Aihara et al., 2008). After final washing, sections were protected with cover slips with anti-fading mounting medium sealed with nail polish and stored at 4°C for preservation.

Cell death was also examined by staining sections by TUNEL using the DeadEnd™ Flurometric TUNEL system according to the manufacturer's protocol (Promega, WI). Slides were then counter-stained with DAPI, washed and coverslipped as described above.

4.3 Immunofluorescence Imaging

This was performed on a confocal microscope (Axiovert 200, Carl Zeiss, Hawthorn, PA) with a charge-coupled device (CCD) camera (Orca AG-CCD, Hamamatsu, Hamamatsu City, Japan). Acquisition parameters (exposure time, laser power strength and pin hole size) were consistent for all sections from each session of staining. Five random images from the right and left sides of each section were photographed for a total of 10 images for each brain area studied (hippocampus, cerebral cortex, brainstem). For double-stained sections, images from the same area were taken under the 2 appropriate wavelengths and the images merged (Image J, National Institutes of Health [NIH], Bethesda, USA).

4.4 Quantification of Neurons and Astrocytes

The number of neurons staining with NeuN were counted using unbiased counting rules by 2 viewers blinded to the experimental group who counted all the cells stained in each photographed field (Mayhew and Gundersen, 1996). Neurons showing positive staining for both NeuN and caspase-3 in double-stained sections were counted as apoptotic. Counting of one slice from each side of the brain was summed to represent that area from each animal.

For GFAP, there was more diffuse staining that made it difficult to accurately count the number of astrocytes. Instead, we quantified the total GFAP positive area and the total overlapping area of GFAP/caspase-3 staining from each section using methods similar to those described by others (bdel-Rahman et al., 2004). This was taken to represent the total number of astrocytes and of apoptotic astrocytes, respectively. Quantification was done using the threshold and mask functions of Image J (NIH). All images were viewed under a microscope at the same light intensity and images captured using one camera setting. A single threshold (to eliminate background noise) was applied to all images based on selection of what appeared as

intracellular specific GFAP staining in several control sections and areas of higher intensity then were taken as being GFAP-positive.

4.5 Statistics

All data were expressed as mean ± standard deviation. Comparisons between groups was performed using Student's t-test or analysis of variance (ANOVA). A $p < 0.05$ was considered significant.

ACKNOWLEDGEMENT

This work was supported by grants (to R.L.M.) from the American Heart Association, the National Institutes of Health (NS25946) and the Brain Research Foundation.

ABBREVIATIONS

ANOVA, analysis of variance; CCD, charge coupled device; DAPI, 4′,6-diamidino-2-phenylindole; GFAP, glial fibrillary acidic protein; NeuN, NeuN; NIH, National Institutes of Health; PBS, phosphate buffered saline; SAH, subarachnoid hemorrhage.

REFERENCES

1. Aihara Y, Jahromi BS, Yassari R, Takahashi M, Macdonald RL. Induction of housekeeping gene expression after subarachnoid hemorrhage in dogs. J. Neurosci. Methods 2008;172:1–7. [PubMed: 18490059]
2. bdel-Rahman A, Rao MS, Shetty AK. Nestin expression in hippocampal astrocytes after injury depends on the age of the hippocampus. Glia 2004;47:299–313. [PubMed: 15293228]
3. Cahill J, Calvert JW, Marcantonio S, Zhang JH. p53 may play an orchestrating role in apoptotic cell death after experimental subarachnoid hemorrhage. Neurosurgery 2007;60:531–545. [PubMed: 17327799]
4. Cahill J, Calvert JW, Solaroglu I, Zhang JH. Vasospasm and p53-induced apoptosis in an experimental model of subarachnoid hemorrhage. Stroke 2006;37:1868–1874. [PubMed: 16741174]
5. Carloni S, Carnevali A, Cimino M, Balduini W. Extended role of necrotic cell death after hypoxia-ischemia-induced neurodegeneration in the neonatal rat. Neurobiol. Dis 2007;27:354–361. [PubMed: 17681771]
6. Corbett D, Nurse S. The problem of assessing effective neuroprotection in experimental cerebral ischemia. Prog. Neurobiol 1998;54:531–548. [PubMed: 9550190]
7. Diringer MN, Heffez DS, Monsein L, Kirsch JR, Hanley DF, Traystman RJ. Cerebrovascular CO2 reactivity during delayed vasospasm in a canine model of subarachnoid hemorrhage. Stroke 1991;22:367–372. [PubMed: 1900646]
8. Dorsch NWC, King MT. A review of cerebral vasospasm in aneurysmal subarachnoid hemorrhage. Part 1: Incidence and effects. Journal of Clinical Neuroscience 1994;1:19–26. [PubMed: 18638721]
9. Endo H, Nito C, Kamada H, Yu F, Chan PH. Reduction in oxidative stress by superoxide dismutase overexpression attenuates acute brain injury after subarachnoid hemorrhage via activation of Akt/glycogen synthase kinase-3beta survival signaling. J. Cereb. Blood Flow Metab 2007;27:975–982. [PubMed: 16969382]
10. Hansen-Schwartz J, Vajkoczy P, Macdonald RL, Pluta RM, Zhang JH. Cerebral vasospasm: looking beyond vasoconstriction. Trends Pharmacol. Sci 2007;28:252–256. [PubMed: 17466386]
11. Haydon PG, Carmignoto G. Astrocyte control of synaptic transmission and neurovascular coupling. Physiol Rev 2006;86:1009–1031. [PubMed: 16816144]
12. Hop JW, Rinkel GJ, Algra A, van Gijn J. Initial loss of consciousness and risk of delayed cerebral ischemia after aneurysmal subarachnoid hemorrhage. Stroke 1999;30:2268–2271. [PubMed: 10548655]

13. Ingall, TJ.; Whisnant, JP. Epidemiology of Subarachnoid Hemorrhage. In: Yanagihara, T.; Piepgras, DG.; Atkinson, JLD., editors. Subarachnoid Hemorrhage. Medical and Surgical Management. Marcel Dekker; New York: 1998. p. 63-78.

14. Jahromi BS, Aihara Y, Ai J, Zhang ZD, Nikitina E, Macdonald RL. Voltage-gated K+ channel dysfunction in myocytes from a dog model of subarachnoid hemorrhage. J. Cereb. Blood Flow Metab 2008;28:797–811. [PubMed: 17987046]

15. Kassell NF, Torner JC, Haley EC Jr. Jane JA, Adams HP, Kongable GL. The International Cooperative Study on the Timing of Aneurysm Surgery. Part 1: Overall management results. J. Neurosurg 1990;73:18–36. [PubMed: 2191090]

16. Macdonald RL, Kakarieka A, Mayer SA, Pasqualin A, Rufenacht DA, Schmiedek P, Kassell NF. Prevention of cerebral vasospasm after aneurysmal subarachnoid hemorrhage with clazosentan, an endothelin receptor antagonist. Neurosurgery 2006;59:453.Abstract

17. Macdonald RL, Pluta RM, Zhang JH. Cerebral vasospasm after subarachnoid hemorrhage: the emerging revolution. Nat. Clin. Pract. Neurol 2007;3:256–263. [PubMed: 17479073]

18. Matz PG, Copin JC, Chan PH. Cell death after exposure to subarachnoid hemolysate correlates inversely with expression of CuZn-superoxide dismutase. Stroke 2000a;31:2450–2459. [PubMed: 11022079]

19. Matz PG, Fujimura M, Chan PH. Subarachnoid hemolysate produces DNA fragmentation in a pattern similar to apoptosis in mouse brain. Brain Res 2000b;858:312–319. [PubMed: 10708682]

20. Mayhew TM, Gundersen HJ. If you assume, you can make an ass out of u and me': a decade of the disector for stereological counting of particles in 3D space. J. Anat 1996;188(Pt 1):1–15. [PubMed: 8655396]

21. Nau R, Haase S, Bunkowski S, Bruck W. Neuronal apoptosis in the dentate gyrus in humans with subarachnoid hemorrhage and cerebral hypoxia. Brain Pathol 2002;12:329–336. [PubMed: 12146801]

22. Nolan CP, Macdonald RL. Can angiographic vasospasm be used as a surrogate marker in evaluating therapeutic interventions for cerebral vasospasm? Neurosurg. Focus 2006;21:E1. [PubMed: 17029333]

23. Ostrowski RP, Colohan AR, Zhang JH. Mechanisms of hyperbaric oxygen-induced neuroprotection in a rat model of subarachnoid hemorrhage. J Cereb. Blood Flow Metab 2005;25:554–571. [PubMed: 15703702]

24. Ouyang YB, Voloboueva LA, Xu LJ, Giffard RG. Selective dysfunction of hippocampal CA1 astrocytes contributes to delayed neuronal damage after transient forebrain ischemia. J. Neurosci 2007;27:4253–4260. [PubMed: 17442809]

25. Park S, Yamaguchi M, Zhou C, Calvert JW, Tang J, Zhang JH. Neurovascular protection reduces early brain injury after subarachnoid hemorrhage. Stroke 2004;35:2412–2417. [PubMed: 15322302]

26. Peterson EW, Cardoso ER. The blood-brain barrier following experimental subarachnoid hemorrhage. Part 1: Response to insult caused by arterial hypertension. J. Neurosurg 1983;58:338–344. [PubMed: 6827318]

27. Prunell GF, Svendgaard NA, Alkass K, Mathiesen T. Delayed cell death related to acute cerebral blood flow changes following subarachnoid hemorrhage in the rat brain. J Neurosurg 2005;102:1046–1054. [PubMed: 16028764]

28. Sasaki T, Kassell NF, Yamashita M, Fujiwara S, Zuccarello M. Barrier disruption in the major cerebral arteries following experimental subarachnoid hemorrhage. J. Neurosurg 1985;63:433–440. [PubMed: 4020472]

29. Stoodley M, Macdonald RL, Weihl CC, Zhang ZD, Lin G, Johns L, Kowalczuk A, Ghadge G, Roos RP. Effect of adenoviral-mediated nitric oxide synthase gene transfer on vasospasm after experimental subarachnoid hemorrhage. Neurosurgery 2000;46:1193–2003. [PubMed: 10807252]

30. Taylor TN, Davis PH, Torner JC, Holmes J, Meyer JW, Jacobson MF. Lifetime cost of stroke in the United States. Stroke 1996;27:1459–1466. [PubMed: 8784113]

31. Wang L, Shi JX, Yin HX, Ma CY, Zhang QR. The influence of subarachnoid hemorrhage on neurons: an animal model. Ann. Clin. Lab Sci 2005;35:79–85. [PubMed: 15830713]

32. Weir B. The pathophysiology of cerebral vasospasm. Br J Neurosurg 1995;9:375–390. [PubMed: 7546359]

33. Xie A, Aihara Y, Bouryi VA, Nikitina E, Jahromi BS, Zhang ZD, Takahashi M, Macdonald RL. Novel mechanism of endothelin-1-induced vasospasm after subarachnoid hemorrhage. J. Cereb. Blood Flow Metab 2007;27:1692–1701. [PubMed: 17392694]

34. Yarnitsky D, Lorian A, Shalev A, Zhang ZD, Takahashi M, Agbaje-Williams M, Macdonald RL. Reversal of cerebral vasospasm by sphenopalatine ganglion stimulation in a dog model of subarachnoid hemorrhage. Surg. Neurol 2005;64:5–11. [PubMed: 15993169]

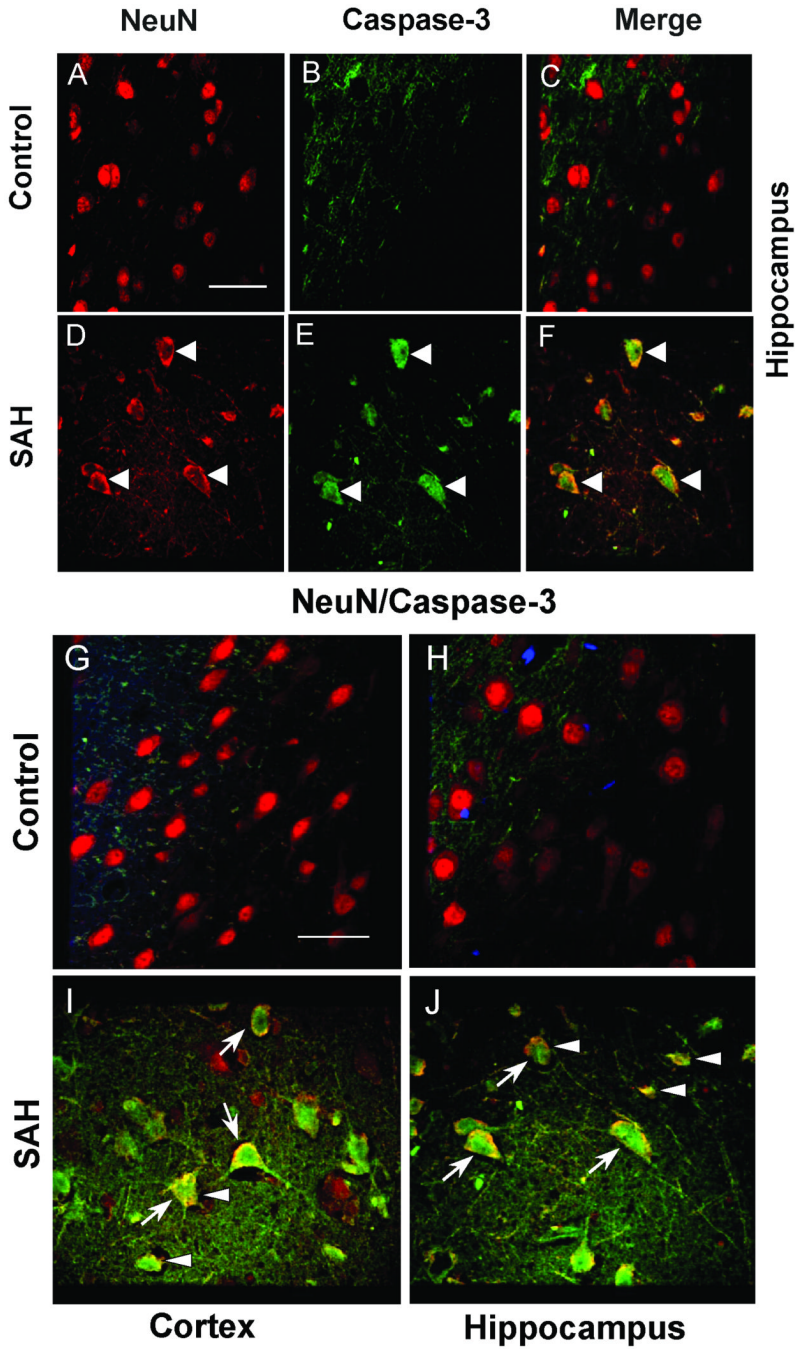

Figure 1. Double-immunofluorescence staining of dog brain for NeuN and active caspase-3

A-F: Images of NeuN-positive (red) cells from control (**A**) and dogs with subarachnoid hemorrhage (SAH, **D**). There were no caspase-3 positive cells in control sections (**B, C**). However, in animals with SAH, cells stained positively for caspase-3 (green, **E**) and they co-localized with NeuN (white arrow heads, **F**). **G-J**: Merged images of NeuN and caspase-3 fluorescence staining from cortex and hippocampus. In both regions, control animals show only NeuN-positive cells (**G, H**), In contrast, animals with SAH show colocalized NeuN/ caspase-3 positive cells (blue arrows, **I, J**). After SAH, shrunken, abnormal cells also can be seen (white arrow heads, **J**). Scale bar = 150 μm.

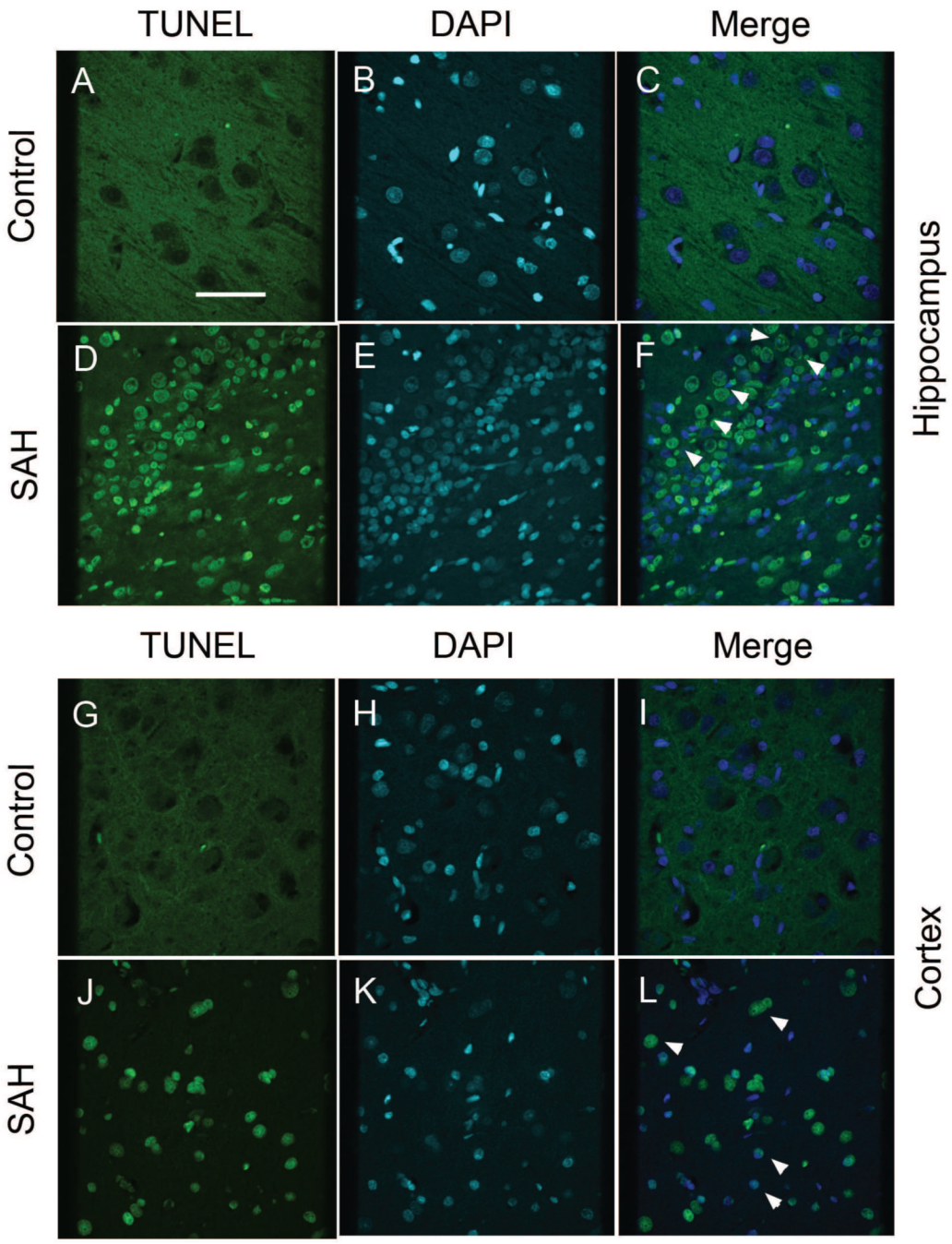

Figure 2. TUNEL staining in hippocampus and cortex of control and SAH dogs

Images of TUNEL-positive (green) cells from control (**A, G**) and dogs with subarachnoid hemorrhage (SAH, **D, J**). Sections are from hippocampus (**A-F**) and cortex (**G-L**). There were no TUNEL-positive cells in control sections (**A, G**). However, in animals with SAH, cells stained positively for TUNEL (green, **D, J**) and co-localized with DAPI nuclear staining (white arrow heads, **F, L**). Scale bar = 150 μm.

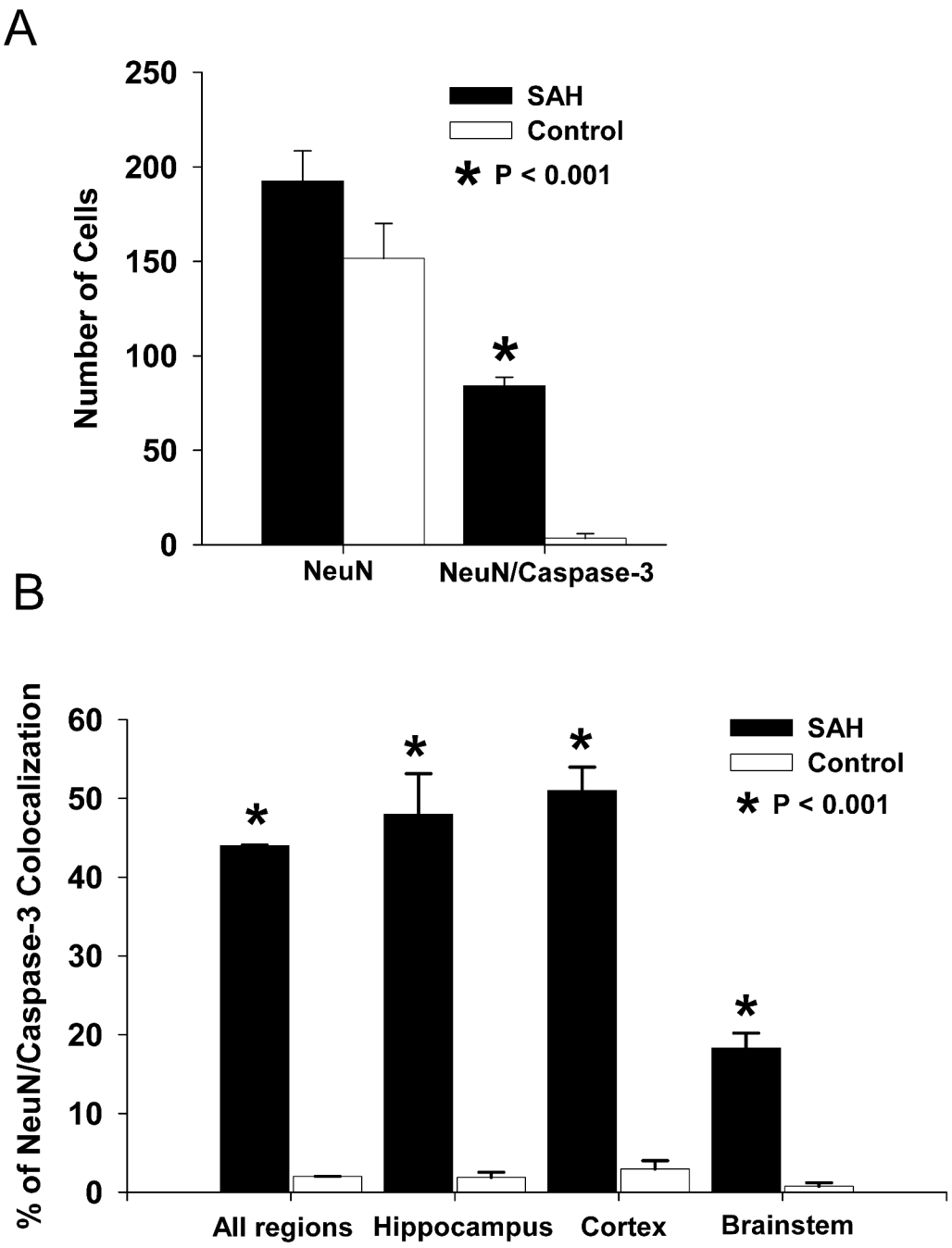

Figure 3. Quantification of NeuN/caspase-3 positive cells in 3 brain areas

A: Bar graph showing no difference between control and SAH groups in the total number of NeuN-positive cells, but a significantly higher number of NeuN/caspase-3 labeled cells in the SAH group. **B**. Bar graph of regional analysis showing a significantly higher percentage of NeuN/caspase-3 co-localization in SAH animals compared to controls in all 3 regions investigated. Values are means ± standard deviations.

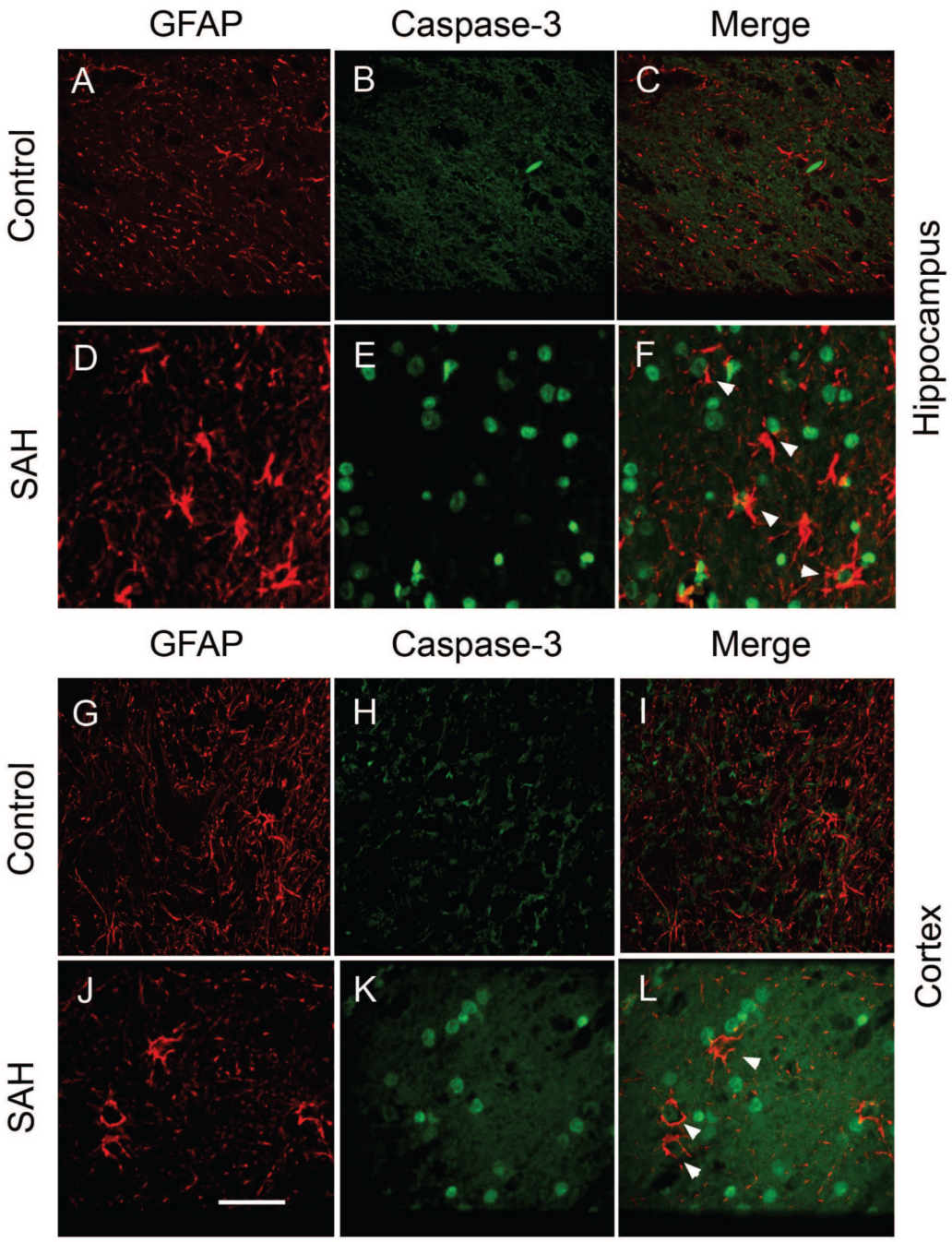

Figure 4. Double immunofluorescence staining of brain sections for GFAP and caspase-3

Representative images showing GFAP (red) and caspase-3 (green) double staining from hippocampus (**A-F**) and cortex (**G-L**). Both regions showed similar patterns of staining. Control animals showed only scant GFAP immunoreactivity (**A, G**) and no caspase-3 staining (**B, H**). In contrast, SAH animals showed marked GFAP staining (**D, J**) and some caspase-3 positive areas (**E, K**) which were co-localized with GFAP (**F, L,** white arrow heads). Scale bar = 150 μm.

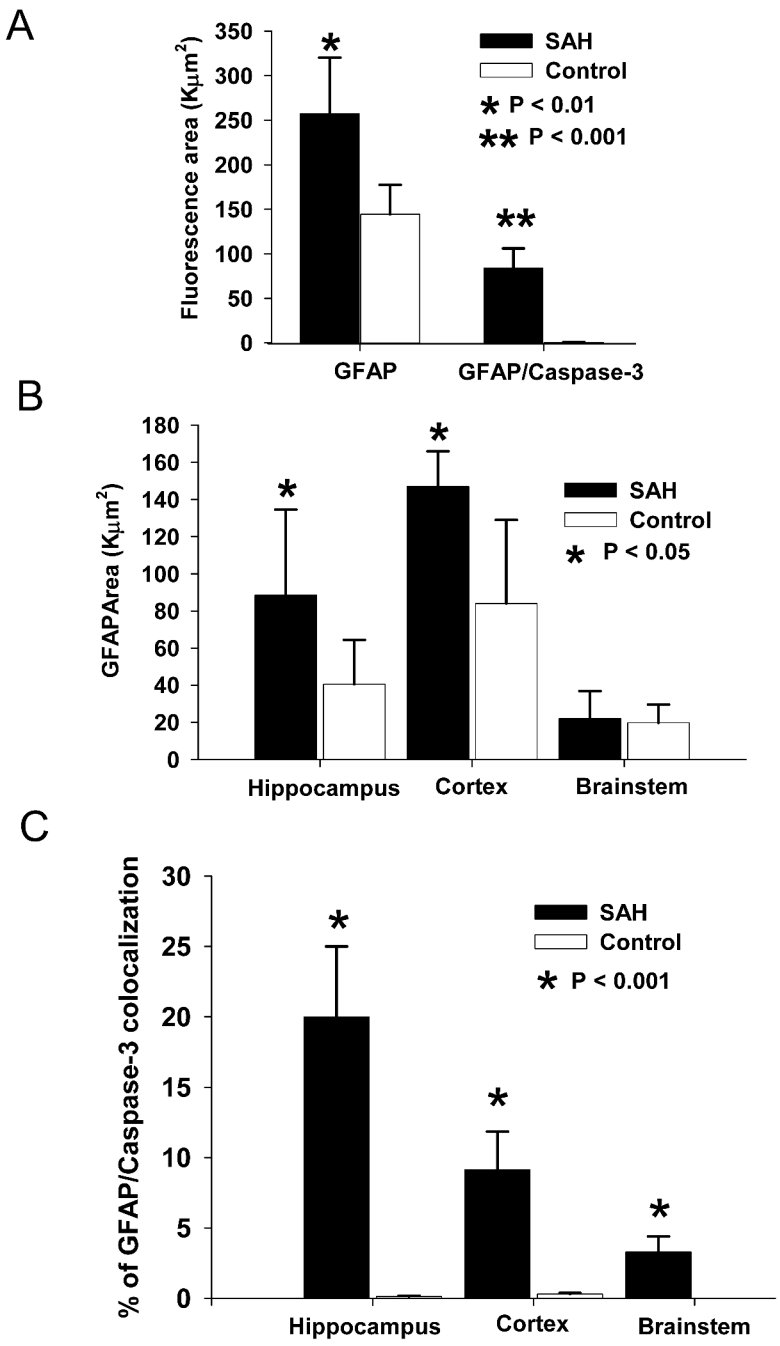

Figure 5. Quantitation of GFAP/caspase-3 immunoreactivity in 3 brain areas

A: Bar graph of fluorescence area showing significant increased total area of GFAP positive staining as well as GFAP/caspase-3 double positive areas in the SAH group compared to controls. **B:** Total GFAP positive stained areas in SAH group were significant larger in hippocampus and cortex, but not brainstem as compared to controls. **C**. The percentage of area showing double immunoreactivity for GFAP and caspase-3 was significantly higher after SAH compared to control in all 3 regions. Values are means ± standard deviations.